



**HAL**  
open science

## Normal butane oxidation: Measurements of autoxidation products in a jet-stirred reactor

Zahraa Dbouk, Nesrine Belhadj, Maxence Lailliau, Guillaume Dayma, Philippe Dagaut, Roland Benoit

► **To cite this version:**

Zahraa Dbouk, Nesrine Belhadj, Maxence Lailliau, Guillaume Dayma, Philippe Dagaut, et al.. Normal butane oxidation: Measurements of autoxidation products in a jet-stirred reactor. *Fuel*, 2023, 350, pp.128865. 10.1016/j.fuel.2023.128865 . hal-04117127

**HAL Id: hal-04117127**

**<https://hal.science/hal-04117127v1>**

Submitted on 6 Jun 2023

**HAL** is a multi-disciplinary open access archive for the deposit and dissemination of scientific research documents, whether they are published or not. The documents may come from teaching and research institutions in France or abroad, or from public or private research centers.

L'archive ouverte pluridisciplinaire **HAL**, est destinée au dépôt et à la diffusion de documents scientifiques de niveau recherche, publiés ou non, émanant des établissements d'enseignement et de recherche français ou étrangers, des laboratoires publics ou privés.

Copyright

# Normal butane oxidation: measurements of autoxidation products in a jet-stirred reactor

Zahraa Dbouk<sup>1,2</sup>, Nesrine Belhadj<sup>1,2</sup>, Maxence Lailliau<sup>1,2</sup>, Roland Benoit<sup>1</sup>, Guillaume Dayma<sup>1,2</sup>, Philippe Dagaut<sup>1</sup>

<sup>1</sup>CNRS-INSIS, ICARE, 1C avenue de la recherche scientifique, 45071 Orleans, France

<sup>2</sup>Université d'Orléans, Château de la Source, avenue du Parc Floral, 45067 Orléans, France

**Correspondence:** philippe.dagaut@cnsr-orleans.fr

**Keywords:** n-butane, oxidation, cool flame, jet-stirred reactor, Orbitrap

## Highlights:

- 37 stable products of oxidation measured by GC and FTIR
- Hydroperoxides and ketohydroperoxides were detected by Orbitrap
- Products of third O<sub>2</sub> addition on fuel's radicals were detected
- Hydroxyl or hydroperoxyl groups in the products were characterized by H/D exchange

## Abstract

The autoxidation of n-butane was studied experimentally in a jet-stirred reactor at 1 atm (560-720 K) and 10 atm (530-1030 K) for an equivalence ratio of 1. Samples of reacting mixtures were analysed in the gas phase by gas chromatography (GC) using several detectors (Flame ionization detector, thermal conductivity detector, quadrupole mass spectrometer), hydrogen peroxide analyser, and Fourier transform infrared spectroscopy. In addition to the fuel and oxygen, 37 products were quantified. Liquid phase samples were obtained by trapping the reacting mixtures in cooled acetonitrile (273 K). The liquid samples were analysed by high resolution mass spectrometry (HRMS Orbitrap Q-Exactive), either after flow injection or separation by high pressure liquid chromatography (HPLC). Besides stable species, several other low-temperature oxidation products, such as hydroperoxides and ketohydroperoxides, were detected. Products of third O<sub>2</sub> addition on fuel's radicals were also detected by high resolution mass spectrometry. To assess the presence of hydroxyl or hydroperoxyl groups in the products of oxidation we performed H/D exchange with D<sub>2</sub>O. Qualitative and quantitative results showed the same trends in terms of variation of mole fractions and signal intensities versus reacting temperature. Kinetic modelling was performed using a literature detailed kinetic reaction mechanism already used to simulate previous n-butane oxidation experiments in the cool-flame regime, showing that improvements are needed to better describe the oxidation of n-butane under the present conditions.

## 34 **1. Introduction**

35 *n*-Butane which has a research octane number of ~ 95 [1] is a minor component of natural gas;  
36 it is also present in liquefied gas from petroleum and gasoline [2]. The autoxidation of *n*-butane  
37 has already been the topic of many studies in the recent years [3-8]. However, few were devoted  
38 to the measurement or detection of elusive intermediate products of cool flames. *n*-Butane  
39 autoxidation has been studied in a jet-stirred reactor (JSR) at atmospheric pressure with  
40 molecular beam mass spectrometry and synchrotron vacuum UV photoionization [9]. The  
41 authors reported the variation of the formation of C<sub>4</sub>-keto hydroperoxides (KHP), C<sub>1</sub>-, C<sub>2</sub>-, and  
42 C<sub>4</sub>-hydroperoxides. Barhini et al. [5, 6] measured concentration profiles of hydrogen peroxide  
43 by cavity ring down spectroscopy (CRDS) in a JSR at atmospheric pressure. Blocquet et al. [8]  
44 measured the mole fractions of the hydroperoxyl radical in a JSR at atmospheric pressure using  
45 the indirect fluorescence assay by gas expansion technique. Djehiche et al. [4] measured  
46 directly the mole fractions of hydrogen peroxide and hydroperoxyl radicals in a JSR at  
47 atmospheric pressure. The experiments of Barhini et al. [5] were simulated by Ranzi et al. [10]  
48 who considered the Korcek mechanism which transforms  $\gamma$ -keto hydroperoxides into acids and  
49 carbonyl products through isomerization and decomposition [10-16]. In the case of *n*-butane,  
50 formic acid + acetone and acetic acid + acetaldehyde are expected products. However, none of  
51 these previous experimental works investigated the formation of products from a third O<sub>2</sub>  
52 addition on fuel's radicals, which has been demonstrated to occur several times in the recent  
53 literature for a range of fuels including alkanes, aldehydes, esters, and ethers [17-28], and no  
54 isomer-resolved data have been reported so far for C<sub>4</sub>-KHPs.

55 In the present work, we performed a series of *n*-butane oxidation experiments in a JSR  
56 at atmospheric pressure to complement those published earlier by Djehiche et al. [4]. Therefore,  
57 we operated under identical conditions of pressure, equivalence ratio, initial fuel mole fraction  
58 and residence time. We studied the formation of cool flame products, including products of  
59 third oxygen addition on fuel's radicals over a range of temperatures under these conditions.  
60 Quantification of chemical products was performed by gas chromatography and Fourier  
61 transform infrared spectroscopy. Experiments were also performed at 10 atm in a JSR where  
62 hydrogen peroxide and a large set of cool flame products were quantified using a range of  
63 analytical techniques. These experiments served to verify the quality of simulated results  
64 obtained using a reaction mechanism taken from the literature.

65

## 66 **2. Experimental**

67 The experiments were performed using a set-up allowing to study the oxidation of *n*-butane  
68 from 1 to 10 atm. A fused silica spherical JSR with a volume of 37 cm<sup>3</sup> was used. There, the  
69 stirring is achieved by 4 jets exiting 0.5 mm i.d. injectors nozzles. Details can be found in  
70 previous publications [29-31]. The mean residence time inside the reactor was 1.4 s at 10 atm  
71 and 6 s at 1 atm. These conditions were chosen in order to get enough fuel-conversion and be  
72 able to observe specific cool flame products. Previous work involved CRDS-GC-FTIR  
73 experiments performed at 6 s residence time in a JSR having the same geometry as that used  
74 here [4]. Also, a similar reactor was used earlier where a range of fuels were oxidized at  
75 residence times in the range 2-4 s [17, 32-35]. No mixing issue was noticed in these previous  
76 works. The temperature along the main axis of the reactor was measured by a movable Pt/Pt-  
77 Rh 10% thermocouple (0.1 mm in diameter) located inside a thin-wall fused silica housing.  
78 Temperature gradient was measured to be ~ 2 K.cm<sup>-1</sup> (see Supporting Material, Fig. S1).

79 High-purity reactants from Air Liquide were oxygen (99.995% pure) and *n*-butane  
80 (>99.5% pure). They were diluted with nitrogen from Air Liquide (<5 ppm H<sub>2</sub>, <50 ppm O<sub>2</sub>,  
81 <100 ppm H<sub>2</sub>O, <1000 ppm Ar) and mixed just before entering the injectors. For the 10 atm  
82 experiments, a cylinder containing 1% of *n*-butane in N<sub>2</sub> (Air Liquide) was used. The *n*-  
83 butane/nitrogen mixture was injected through a capillary and the O<sub>2</sub>/N<sub>2</sub> mixture flowed in the  
84 reactor extension tube [31]. Mass flow controllers (Brooks 5850TR) were used for gas delivery.  
85 The gases were preheated before injection in the reactor to minimize temperature gradients  
86 inside the JSR. The experimental conditions are summarized in Table 1.

87

88 **Table 1.** Experimental conditions.

Parameters	1 atm experiments	10 atm experiments
Temperature range (K)	560-720	530-1030
Mean residence time (s)	6	1.4
Equivalence ratio	1	1
Initial mole fraction of <i>n</i> -butane	0.023	0.004
Initial mole fraction of O <sub>2</sub>	0.1495	0.026

89

90 Mole fractions of reactants and stable species formed during the autoxidation of *n*-  
91 butane at 1 and 10 atm were obtained using several instruments (gas chromatography with flame  
92 ionization detection–FID, thermal conductivity detection–TCD, and benchtop mass  
93 spectrometry–MS, online Fourier transform infrared spectroscopy–FTIR, online ATI hydrogen

94 peroxide dual-channel monitor at 10 atm). The gas samples taken with a sonic probe were  
95 analysed online by FTIR and stored at 50 mbar in 1 L Pyrex bulbs for off-line gas  
96 chromatography analyses. For GC and FTIR analyses, uncertainties on mole fractions were ca.  
97 15%. For ATI analyses of H<sub>2</sub>O<sub>2</sub>, uncertainties on mole fractions were < 20 %.

98 In addition, for the autoxidation experiments at 1 atm, samples were taken by bubbling  
99 oxidation samples in 20 mL of cool acetonitrile (0°C) for 75 min. The solution obtained was  
100 analysed by flow injection (FIA) - Orbitrap Q-Exactive and liquid chromatography - Orbitrap  
101 Q-Exactive. Two ionisation sources were used in positive and negative modes, i.e., atmospheric  
102 pressure chemical ionisation (APCI) and heated electrospray ionisation (HESI). A HPLC  
103 column (Acentis silica column from Supelco, 5µm, 100 Å, 250x2.1 mm) was used with an  
104 acetonitrile-water solvent (82.5% acetonitrile and 17.5% water). This procedure providing  
105 qualitative data is described at length in previous publications [18-20, 23, 25-27]. Because  
106 Orbitrap Q-Exactive cannot detect ions at  $m/z < 50$ , M-HCOO<sup>-</sup> adduct ions were recorded. That  
107 way, H<sub>2</sub>O<sub>2</sub> and C<sub>1</sub>-C<sub>3</sub> products (CH<sub>2</sub>O, CH<sub>2</sub>O<sub>2</sub>, C<sub>2</sub>H<sub>4</sub>O) were analysed. Ketohydroperoxides,  
108 butyl hydroperoxides or diols and diketones were analysed as a function of temperature, and  
109 products of third O<sub>2</sub> addition on fuel's radicals were detected. To assess the presence of OOH  
110 and/or OH functional groups in the products of oxidation, we performed OH/OD exchange.  
111 Here, 300 µL of D<sub>2</sub>O (99.98% from Sigma-Aldrich) were introduced into 1 mL of liquid  
112 samples. We let H/D exchange to proceed for 20 min before analyses.

113

### 114 **3. Kinetic modelling**

115 Kinetic modelling was performed using the Chemkin software [36]. We used the semi-detailed  
116 chemical kinetic reaction mechanism from Ranzi et al. [10] which takes into account the Korcek  
117 mechanism converting  $\gamma$ -ketohydroperoxides into acids and carbonyls. In that mechanism,  
118 butyl hydroperoxides, butyl ketohydroperoxides and cyclic ethers are represented by a single  
119 specie (C<sub>4</sub>H<sub>9</sub>OOH, NC<sub>4</sub>-OQOOH, C<sub>4</sub>H<sub>8</sub>O, respectively). The measured temperatures in JSR  
120 experiments were used as input in the PSR module for computations.

121

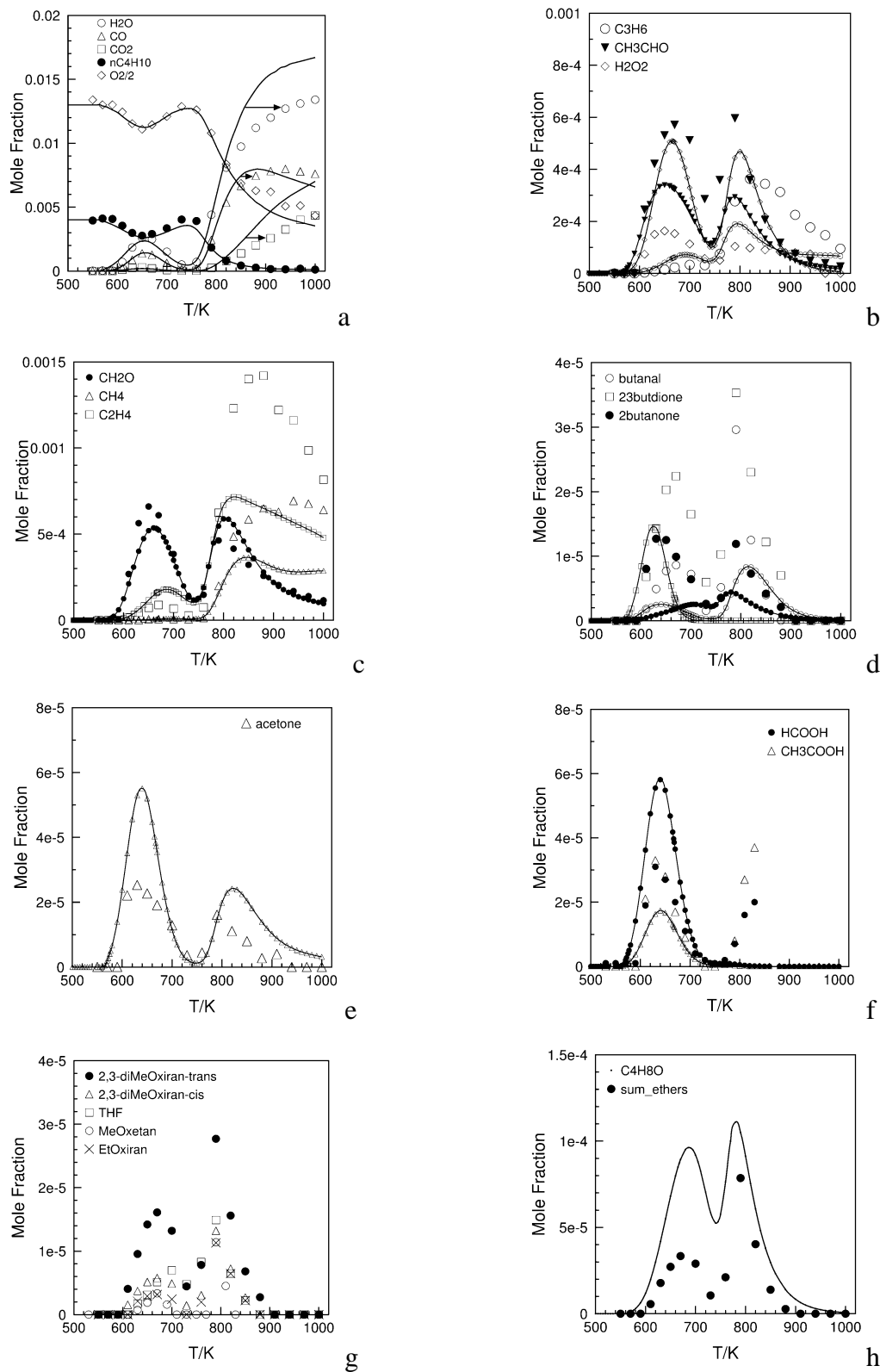
### 122 **4. Results and discussion**

#### 123 4.1 Oxidation at 10 atm

124 The results obtained under high pressure conditions (Table 1) consisted of mole fractions of the  
125 reactants (*n*-butane and oxygen), a large set of stable intermediates, and final products (carbon  
126 dioxide and water). Most of the chemical products were measured by FID after capillary column  
127 separation (50 m alumina column, 30 m and 3µm DB1 – 25 m and 1.2 µm CP-Sil 5CB, and 60

128 m DB624 capillary columns). A TCD was used to measure oxygen and hydrogen after  
129 separation on a 25 m CarboPlot P7 column. FTIR was used to measure CO, CO<sub>2</sub>, acids, and  
130 CH<sub>2</sub>O (temperature-controlled gas cell: 140°C, 10 m pathlength, resolution of 0.5 cm<sup>-1</sup>, 200  
131 mbar of pressure). Calibrations were made by analysing standards. When standards could not  
132 be used in FID analyses, carbon-equivalent rules were applied [37]. Gas chromatography-mass  
133 spectrometry (GC-MS) was used for products identification (electron impact ionization at 70  
134 eV). The quantified chemical species, besides the reactants, were final products and stables  
135 intermediates: H<sub>2</sub>, H<sub>2</sub>O, H<sub>2</sub>O<sub>2</sub>, CO<sub>2</sub>, CO, CH<sub>2</sub>O, CH<sub>4</sub>, C<sub>2</sub>H<sub>2</sub>, C<sub>2</sub>H<sub>4</sub>, C<sub>2</sub>H<sub>6</sub>, oxirane, C<sub>3</sub>H<sub>6</sub>, trans  
136 2-C<sub>4</sub>H<sub>8</sub>, cis 2-C<sub>4</sub>H<sub>8</sub>, 1-C<sub>4</sub>H<sub>8</sub>, 1,3-C<sub>4</sub>H<sub>6</sub>, CH<sub>3</sub>CHO, methyl oxirane, 2-propenal, propanal,  
137 acetone, 2,3-dimethyl oxirane (cis and trans), ethyl oxirane, 2-methyl oxetane, furan, 2,3- and  
138 2,5-dihydrofuran, methacrolein, butanal, 2,3-butanedione, 2-butanone, 3-buten-2-ol, methyl  
139 vinyl ketone, tetrahydrofuran (THF), formic acid, acetic acid. Figures 1a to 1h illustrate the  
140 results and presents a comparison of experimental and simulated mole fraction profiles under  
141 stoichiometric conditions.

142 Figure 1a shows that the model [10] slightly overestimates the oxidation rate of the fuel  
143 in the negative temperature coefficient regime (NTC). Above ca. 850 K, the predicted formation  
144 of carbon dioxide and water is too important. The formation of hydrogen peroxide is too  
145 important in the cool flame, due to overproduction of hydroxyl radicals (Fig. 1b). Figures 1b  
146 and 1c show that the model also tends to strongly overestimate the rate of oxidation of important  
147 intermediates such as ethylene, methane and propene. Acetaldehyde consumption rate above  
148 ca. 700 K is also overpredicted. Concerning carbonyl compounds (Figs. 1d and 1e), the model  
149 overestimates the production of acetone and underestimates that of 2-butanone and butanal. The  
150 formation of 2,3-butanedione is underestimated by a factor of 2 in the cool flame, and not  
151 formed in the simulation above 750 K. Although the fuel conversion is well predicted, acetic  
152 acid computed mole fractions do not match the data in the cool flame (Fig. 1f). Above ca. 800  
153 K, the model does not predict acetic acid formation. Formic acid formation in the cool flame is  
154 overpredicted by a factor of ca. 2. No reaction is included in the kinetic model to explain the  
155 formation of acids at T > 800 K. Their formation through reactions of the corresponding  
156 aldehydes with OH could play a role since formaldehyde and acetaldehyde reach mole fractions  
157 of ca. 500 and 600 ppm, respectively. Several C<sub>4</sub>-cyclic ethers were measured here (Fig. 1g).  
158 In the model, they are represented by a single product, C<sub>4</sub>H<sub>8</sub>O (Fig. 1h). One can see from  
159 Figure 1g that 2,3-dimethyl oxirane is the most important ether formed here. The observed order  
160 of importance is: 2,3-dimethyl oxirane (A) >> tetrahydrofuran (B) ≥ 2-methyloxetane (C) ≈  
161 ethyloxirane (D).

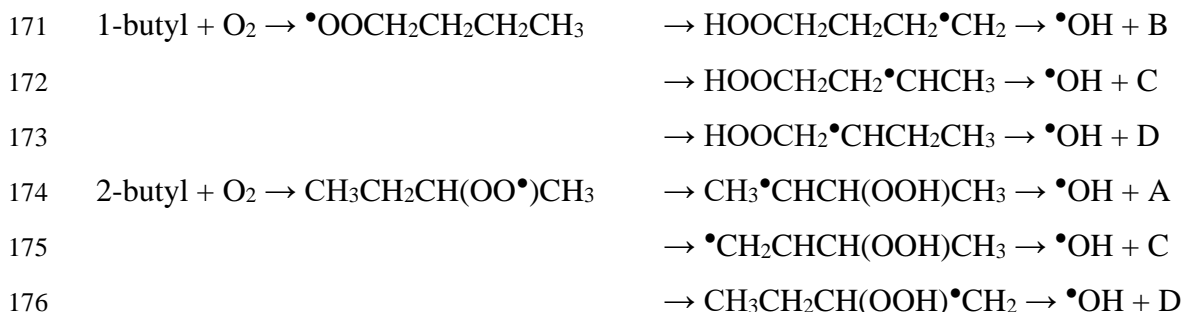


163 **Fig. 1.** Comparison of experimental (symbols) and simulated (lines and small symbols) mole  
 164 fractions of selected species measured during the oxidation of *n*-butane in a JSR under  
 165 stoichiometric conditions at 10 atm (see Table 1).

166

167 The oxidation of 2-butyl can lead to the formation of all these isomers, except THF,  
168 whereas the oxidation of 1-butyl leads to the formation of tetrahydrofuran, 2-methyloxetane,  
169 and ethyloxirane:

170



177

178 The sum of the mole fractions of these ethers was compared to the computed C<sub>4</sub>H<sub>8</sub>O  
179 mole fractions (Fig. 1h). Because the model does not predict a NTC as strong as in the  
180 experiments, it could not fully represent all the data. Whereas pathways other than the Korcek  
181 mechanism could yield acetone, formic acid, acetaldehyde and acetic acid, as noticed at 10 atm  
182 in the cool flame, the two acids are produced in nearly equal quantities similar to acetone.  
183 Acetaldehyde maximum mole fraction is nearly 12 times higher. Reaction pathway analysis  
184 was performed at 640 K, showing that formic acid is produced via nC<sub>4</sub>-OQOOH → HCOOH +  
185 CH<sub>3</sub>COCH<sub>3</sub>, acetaldehyde comes mainly from nC<sub>4</sub>-OQOOH → CH<sub>3</sub>CHO + 0.3 CH<sub>3</sub>CO + 0.7  
186 CH<sub>2</sub>CHO + OH and OH + nC<sub>4</sub>-OQOOH → H<sub>2</sub>O + CH<sub>2</sub>CO + CH<sub>3</sub>CHO + OH (half importance),  
187 acetic acid is formed via nC<sub>4</sub>-OQOOH → CH<sub>3</sub>CHO + CH<sub>3</sub>COOH, and acetone's  
188 overproduction is due to nC<sub>4</sub>-OQOOH → HCOOH + CH<sub>3</sub>COCH<sub>3</sub>.

189 In summary, the model proposed by Ranzi et al.[10] describes only a fraction of the  
190 present 10 atm data whereas it was previously shown to represent data obtained at atmospheric  
191 pressure. Nevertheless, we further used that mechanism for simulating experiments performed  
192 at 1 atm (Section 4.2).

193

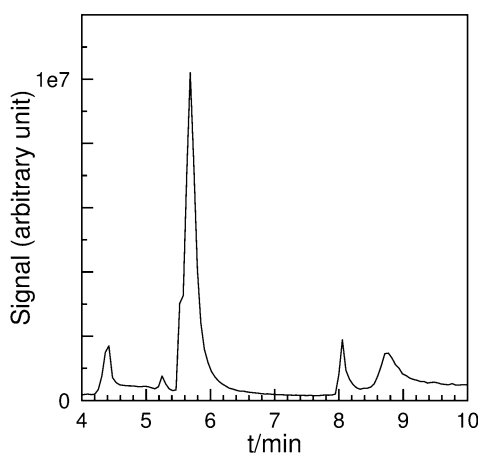
#### 194 4.2 Oxidation at 1 atm

195 In addition to chromatographic and FTIR analyses (see Section 3.1 for details),  
196 qualitative analyses were made by Orbitrap. They consisted of ions signal profiles obtained for  
197 samples taken as a function of JSR temperature and constant residence time. FIA and HPLC  
198 were used. M-HCOO<sup>-</sup> adduct ions were recorded (APCI in negative ionisation mode) for low-  
199 mass products: H<sub>2</sub>O<sub>2</sub>, CH<sub>2</sub>O, C<sub>2</sub>H<sub>4</sub>O. Ketohydroperoxides (KHP, C<sub>4</sub>H<sub>8</sub>O<sub>3</sub>) and isomers,



200 butylhydroperoxides ( $C_4H_{10}O_2$ ) and isomers, cyclic ethers and isomers ( $C_4H_8O$ ) and  
 201 butanediones ( $C_4H_6O_2$ ) resulting from ketohydroperoxides decomposition were measured, as  
 202 well as  $C_4H_8O_5$ , produced via third  $O_2$  addition on fuel's radicals (Table 2). That last product  
 203 was too low in concentration to present data as a function of JSR temperature. The formation  
 204 of ketohydroperoxides occurs via the addition of two molecules of oxygen on the fuel's radicals:  
 205  $C_4H_9\bullet + O_2 \rightarrow C_4H_9OO\bullet$  followed by H-atom transfer yielding  $\bullet C_4H_8OOH$  which reacts with  
 206 oxygen and, after H-atom transfer, decomposes to form a KHP, i.e.,  $\bullet C_4H_8OOH + O_2 \rightarrow$   
 207  $\bullet OOC_4H_8OOH \rightarrow \bullet C_4H_7(OOH)_2 \rightarrow C_4H_8O_3 + \bullet OH$ . Six different KHPs can be produced during  
 208 the oxidation of *n*-butane. Our HPLC-Orbitrap APCI (-) analyses demonstrated the presence  
 209 of a major chromatographic peak and of four other lower intensity peaks (Fig. 2). Coelution of  
 210 the main chromatographic peak could not be avoided. It could be due to KHPs arising from the  
 211 peroxidation of 1-butyl and 2-butyl radicals, i.e.,  $CH_3(C=O)CH_2CH_2OOH$  and  
 212  $CH_3CH(OOH)CH_2CH(=O)$ , respectively. The isomers could not be identified due to the  
 213 formation of too similar fragments (fragmentation energy of 10 eV). However, kinetic  
 214 modelling using an in-house detailed scheme [38] predicted the above mentioned KHPs being  
 215 dominant ( $CH_3(C=O)CH_2CH_2OOH > CH_3CH(OOH)CH_2CH(=O)$ ).

216



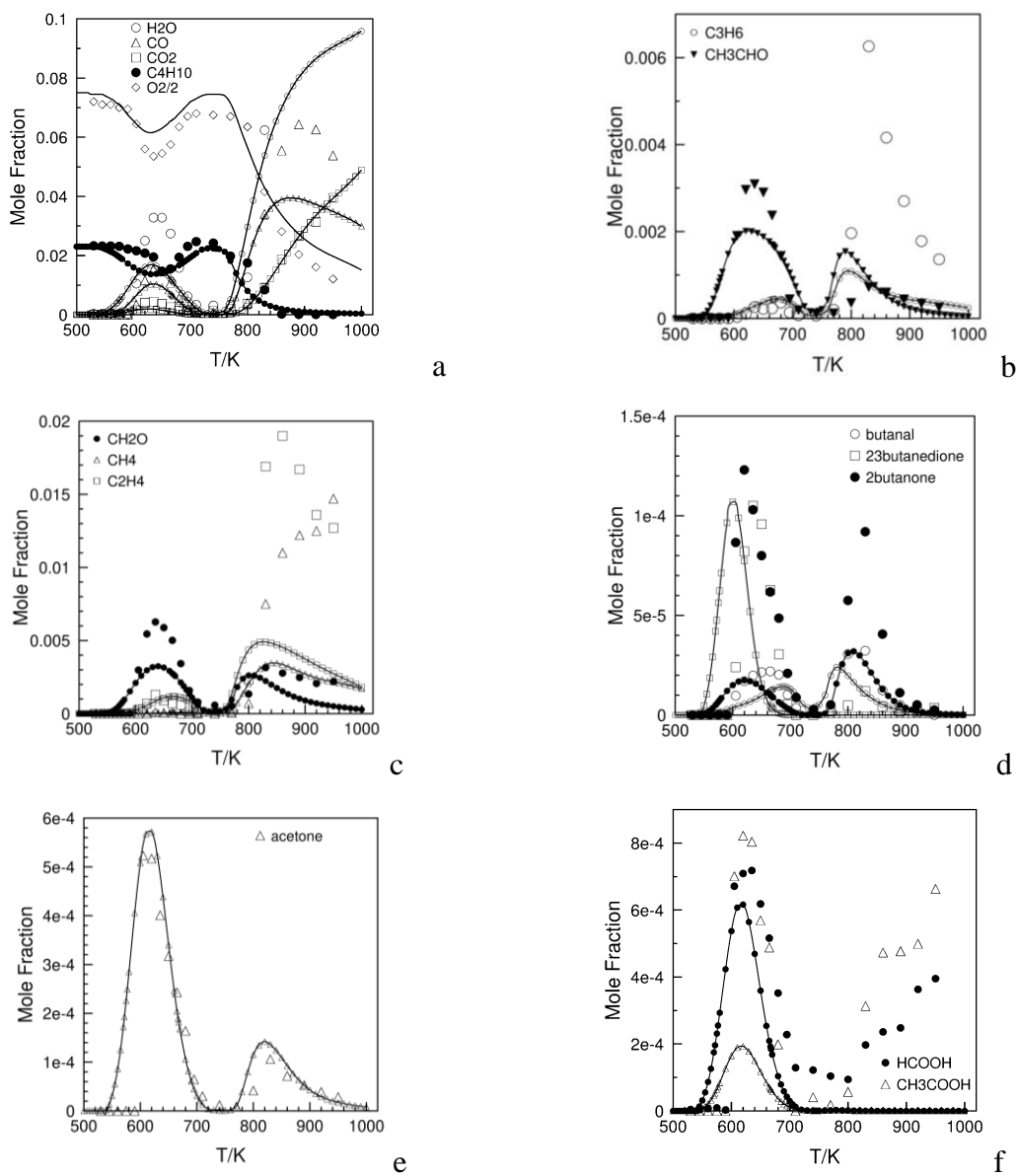
217

218 **Fig. 2.** Separation of ketohydroperoxides by liquid chromatography and detection by Orbitrap.  
 219 Sample taken at 1 atm, 600 K. APCI (-) was used; ionic signal at  $m/z$  103.03880. is plotted.

220

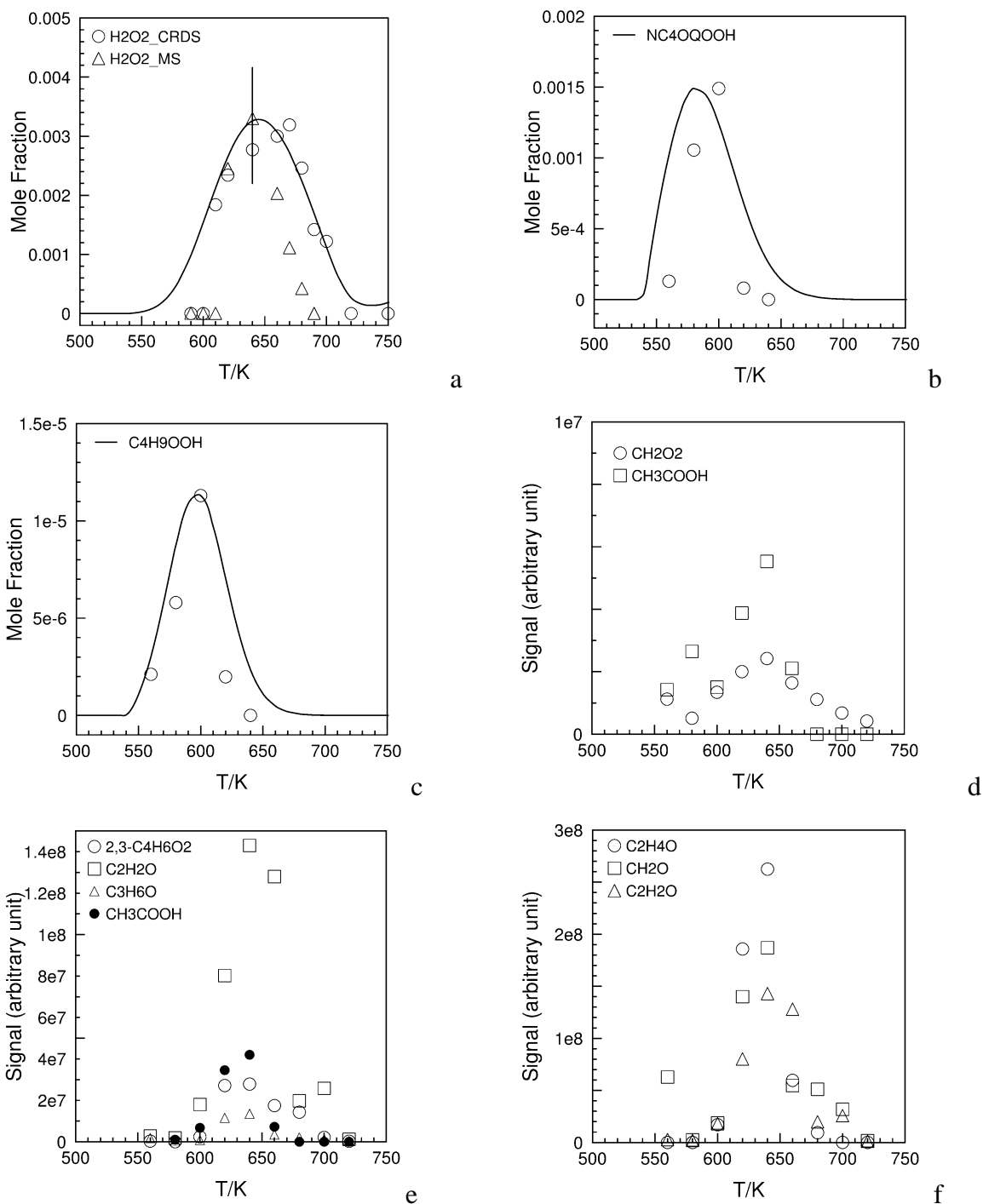
221 Figures 3 and 4 present the experimental results obtained here. When possible, the  
 222 present data are compared to (i) our previous data obtained by CRDS and (ii) modelling results.  
 223 Figure 3a shows that the model overestimates the fuel oxidation rate below 700 K although the  
 224 formation of water is underestimated in the cool flame. The production of  $CO$  and  $CO_2$  is also  
 225 underestimated by the model in the cool flame. Above 800 K, the model better represents the

226 data. Figures 3b and 3c show that formation of formaldehyde and that of acetaldehyde are  
 227 underestimated by the model in the cool flame.  
 228



229 **Fig. 3** Comparison of experimental (symbols) and simulated (lines and small symbols) mole  
 230 fractions of selected species measured during the oxidation of *n*-butane in a JSR under  
 231 stoichiometric conditions at 1 atm (see Table 1).

232  
 233



234 **Fig. 4.** Comparison of experimental data (symbols) and simulated mole fractions (lines) of  
 235 selected species measured during the oxidation of *n*-butane in a JSR under stoichiometric  
 236 conditions at 1 atm (see Table 1). Only CRDS data are quantitative in Fig. 4a. MS data were  
 237 scaled to the maximum computed mole fraction.

238  
 239 Above 800 K, discrepancies between data and simulated mole fraction are observed for  
 240 all the intermediate products. Figure 3e presents the results obtained for acetone and Fig. 3d  
 241 presents those for C<sub>4</sub>-carbonyls. One can see that acetone formation is well predicted over the

242 entire temperature range of this study. The production of 2,3-butanedione and that of butanal  
243 are predicted well, but the model fails to predict the formation of 2-butanone (17.5 ppm  
244 predicted at 620 K vs. 123 ppm measured at 620 K). On Figure 3f, products of the Korcek  
245 mechanism are plotted. Whereas other routes than the Korcek mechanism can yield acetone,  
246 formic acid, acetaldehyde and acetic acid, it is interesting to note that in the cool flame, the two  
247 acids are produced in nearly equal quantities, also very close to that of acetone. Acetaldehyde  
248 maximum mole fraction is c.a. 4 times higher. In the cool flame, the formation of formic acid  
249 is well predicted whereas that of acetic acid is underestimated by a factor of ca. 4. At 600 K, a  
250 rate of production analysis was performed. It indicated that formic acid comes from the  
251 decomposition of C<sub>4</sub> KHPs:  $n\text{C}_4\text{-OQOOH} \rightarrow \text{HCOOH} + \text{CH}_3\text{COCH}_3$  (Korcek mechanism). In  
252 the model, acetaldehyde is mainly formed by two reactions of equal importance:  $n\text{C}_4\text{-OQOOH}$   
253  $\rightarrow \text{CH}_3\text{CHO} + 0.3 \text{CH}_3\text{CO} + 0.7 \text{CH}_2\text{CHO} + \text{OH}$  and  $n\text{C}_4\text{-OQOOH} \rightarrow \text{H}_2\text{O} + \text{CH}_2\text{CO} +$   
254  $\text{CH}_3\text{CHO} + \text{OH}$ . In the computations, acetic acid is formed through the decomposition of C<sub>4</sub>-  
255 KHPs:  $n\text{C}_4\text{-OQOOH} \rightarrow \text{CH}_3\text{CHO} + \text{CH}_3\text{COOH}$  (Korcek mechanism). In the simulations,  
256 acetone is essentially formed through the decomposition of C<sub>4</sub>-KHPs:  $n\text{C}_4\text{-OQOOH} \rightarrow$   
257  $\text{HCOOH} + \text{CH}_3\text{COCH}_3$  (Korcek mechanism).

258 Figure 4 presents the HRMS data compared to simulations for selected products. In Fig.  
259 4a, HRMS data were scaled to CRDS data at 640 K; analyses were performed using HPLC-  
260 HRMS APCI (-); the signal corresponds to m/z 79.0022 for H<sub>2</sub>O<sub>2</sub> with HCOO<sup>-</sup> adduct. In Fig.  
261 4b, HRMS data were scaled to simulated maximum mole fraction. Analyses were carried out  
262 by FIA- APCI (+); the signal at m/z 105.05484 is plotted. In Fig. 4c, HRMS data were scaled  
263 to simulations. Analyses were performed by FIA-APCI (+); the signal at m/z 91.07576 is  
264 plotted. In Fig. 4d to 4f, raw ionic signals are presented. In Fig. 4d, CH<sub>2</sub>O<sub>2</sub> is detected with a  
265 HCOO<sup>-</sup> adducts. Analyses of CH<sub>2</sub>O<sub>2</sub> were performed using HPLC-HRMS APCI (-); the signal  
266 at m/z 91.0021 is plotted. For CH<sub>3</sub>COOH analysis, we used HESI (-) HPLC-HRMS; the signal  
267 at m/z 59.0124 is presented. In Fig. 4e C<sub>2</sub>H<sub>2</sub>O and CH<sub>3</sub>COOH are detected with HCOO<sup>-</sup>  
268 adducts. The analyses of C<sub>2</sub>H<sub>2</sub>O were carried out using APCI (-) HPLC-HRMS (signal at m/z  
269 87.0072). The analyses of C<sub>4</sub>H<sub>6</sub>O<sub>2</sub> and C<sub>3</sub>H<sub>6</sub>O were performed using APCI (+) HPLC-HRMS  
270 (signal at m/z 87.0447 and m/z 59.0500, respectively). The analysis of CH<sub>3</sub>COOH was  
271 performed by HESI (-) HPLC-HRMS (signal at m/z 105.0176).

272 In Fig. 4f, C<sub>2</sub>H<sub>4</sub>O, CH<sub>2</sub>O, and C<sub>2</sub>H<sub>2</sub>O were detected with HCOO<sup>-</sup> adducts using APCI  
273 (-) HPLC-HRMS (signal at m/z 89.0228, m/z 75.0072, and m/z 87.0072, respectively). Figure  
274 4a shows a comparison of quantitative measurements of hydrogen peroxide by CRDS [4],  
275 qualitative HRMS measurement, and computed mole fractions using the model of Ranzi et al.

276 The HRMS data were scaled to the CRDS data at 640 K. One can see good agreement between  
277 all the mole fraction profiles. Figure 4b shows the simulated KHP mole fractions compare to  
278 HRMS data scaled to the maximum computed mole fraction. From that figure, one can observe  
279 a good match between data and modelling. This is also the case for  $C_4H_{10}O_2$   
280 (butylhydroperoxides and diols) when HRMS data are scaled to the maximum computed mole  
281  $C_4H_9OOH$  fraction. APCI and HESI were used to track a set of other species. The present results  
282 are presented in Figures 4d, e, f. From these figures, one can see that all the products present a  
283 maximum signal intensity at 640 K, as observed in corresponding GC analyses of most of the  
284 intermediate cool flame products. Molecular formulae can correspond to several isomers, e.g.,  
285  $C_2H_4O$ . However, one can estimate that  $CH_2O_2$  represents formic acid,  $CH_2O$  represents  
286 formaldehyde,  $C_2H_2O$  represents ketene,  $C_2H_4O_2$  represents acetic acid,  $C_3H_6O$  represents  
287 mostly acetone, and  $C_2H_4O$  represents mainly acetaldehyde (~64% acetaldehyde and ~36%  
288 oxirane as determined by GC analyses). The profile for 2,3- $C_4H_6O_2$  was obtained by HPLC-  
289 HRMS after identification using a 2,3-butanedione standard.

290 In order to further characterise the cool flame products, we performed H/D exchange  
291 with  $D_2O$  to assess the presence of hydroxyl or hydroperoxyl groups in the products (Table 2).  
292 Analyses were performed in FIA/APCI (+/-) modes. For KHPs ( $C_4H_8O_3$ ) a strong H/D  
293 exchange was observed as shown in Table 2. Indeed, after addition of  $D_2O$ , one measured  
294 signals with intensities of  $7.32E+6$ ,  $1.16E+7$ , and  $7.14E+6$  for  $D_0$ ,  $D_1$ , and  $D_2$  products,  
295 respectively. The  $D_2$  exchange should indicate the presence of ketodiols.

296  $C_4H_6O_2$  corresponds to several isomers. Butanediones were identified by GC-MS.  
297 Because two H/D exchanges were observed here, unsaturated diols are likely present in the  
298 analysed sample. Many isomers can correspond to  $C_4H_8O$ . In this work, cyclic ethers, ketones,  
299 aldehydes, and unsaturated alcohols have been identified by GC-MS. Among this species, only  
300 unsaturated alcohols could form deuterated products in presence of  $D_2O$ . Here, the observation  
301 of  $C_4H_7D_1O$  indicates their likely presence in the oxidation products.  $C_4H_8O_2$  could represent  
302 butyric acid and unsaturated hydroperoxides. Because  $C_4H_7D_1O_2$  was observed, the presence  
303 of unsaturated ROOH in the analysed sample is likely since the butyric acid isomeric form  
304 shows no H/D exchange in presence of  $D_2O$  [18].  $C_4H_{10}O_2$  can represent diols and ROOH. The  
305 strong signal observed for  $C_4H_8D_2O_2^+$  indicates the likely presence of diols in the sample.  
306 Indeed, after addition of  $D_2O$ , one measured signals with intensities of  $9.45E+6$ ,  $1.06E+7$ , and  
307  $3.25E+6$  for  $D_0$ ,  $D_1$ , and  $D_2$  products, respectively. The major H/D exchange yields  $D_1$  products  
308 whereas the  $D_2$  exchange represents 1/3 of  $D_0$  or  $D_1$  signals which should indicate the presence  
309 of two OH groups in  $C_4H_{10}O_2$ .

310

311

312 **Table 2.** H/D exchange results for products of *n*-butane oxidation in a JSR at 640K and 1 atm.

M (g/mol)	Species		APCI (+)		APCI (-)	
	Formula	Possible isomers	<i>m/z</i> (M+H) <sup>+</sup>	Signal (a.u)	<i>m/z</i> (M-H) <sup>-</sup>	Signal (a.u)
72	C <sub>4</sub> H <sub>8</sub> O	cyclic ether ketones aldehydes unsaturated alcohol	73.06538	1.02E8	71.04977	2.87E5
73	C <sub>4</sub> H <sub>7</sub> D <sub>1</sub> O	unsaturated alcohol	74.07173	8.90E7	72.05535	4.11E4
86	C <sub>4</sub> H <sub>6</sub> O <sub>2</sub>	dione or unsaturated diols	87.04385	2.93E8	85.02824	5.59E6
87	C <sub>4</sub> H <sub>5</sub> D <sub>1</sub> O <sub>2</sub>	unsaturated diols	88.05024	4.32E7	86.03459	5.18E6
88	C <sub>4</sub> H <sub>4</sub> D <sub>2</sub> O <sub>2</sub>	unsaturated diols	89.05715	1.80E7	87.04084	8.90E4
88	C <sub>4</sub> H <sub>8</sub> O <sub>2</sub>	butyric acid or unsaturated ROOH	89.06010	2.38E7	87.04451	3.34E5
89	C <sub>4</sub> H <sub>7</sub> D <sub>1</sub> O <sub>2</sub>	<i>idem</i>	90.06646	2.30E7	88.05024	3.60E5
90	C <sub>4</sub> H <sub>6</sub> D <sub>2</sub> O <sub>2</sub>	<i>idem</i>	91.07281	2.46E6	89.05647	2.51E5
90	C <sub>4</sub> H <sub>10</sub> O <sub>2</sub>	ROOH or diols	91.07575	9.45E6	89.05959	1.95E5
91	C <sub>4</sub> H <sub>9</sub> D <sub>1</sub> O <sub>2</sub>	<i>idem</i>	92.08211	1.06E7	-	-
92	C <sub>4</sub> H <sub>8</sub> D <sub>2</sub> O <sub>2</sub>	diols	93.08837	3.25E6	-	-
104	C <sub>4</sub> H <sub>8</sub> O <sub>3</sub>	KHPs or keto-diols	105.05444	7.32E6	103.03880	7.67E7
105	C <sub>4</sub> H <sub>7</sub> D <sub>1</sub> O <sub>3</sub>	KHPs or keto-diols	106.06120	1.16E7	104.04517	7.77E7
106	C <sub>4</sub> H <sub>6</sub> D <sub>2</sub> O <sub>3</sub>	keto-diols	107.0674	7.14E6	105.05139	5.40E4
136	C <sub>4</sub> H <sub>8</sub> O <sub>5</sub>	keto-dihydroperoxide	137.04578	1.54E4	135.02859	2.01E5
137	C <sub>4</sub> H <sub>7</sub> D <sub>1</sub> O <sub>5</sub>	<i>idem</i>	-	-	136.03522	9.41E5
138	C <sub>4</sub> H <sub>6</sub> D <sub>2</sub> O <sub>5</sub>	<i>idem</i>	-	-	137.04152	9.84E5

313  
 314 If the second H-atom transfer in a peroxy-alkylhydroperoxide radical does not occur on  
 315 the C-atom bonded to the OOH group, a third O<sub>2</sub> addition can occur and yield a keto-alkyl-  
 316 dihydroperoxide:



319 Only a small signal of the corresponding ion  $C_4H_9O_5^+([M+H]^+)$  was observed under the  
320 present conditions with positive APCI ionisation. We performed H/D exchange with  $D_2O$  to  
321 verify the presence of two hydroperoxyl groups in  $C_4H_8O_5$ . As can be seen from Table 2,  
322  $C_4H_5D_2O_5^-([M-H]^-)$  could be observed, confirming the formation of a keto-alkyl-  
323 dihydroperoxide.

324

## 325 **5. Conclusion**

326 New experimental results were obtained in a JSR at 1 and 10 atm, using a range of analytical  
327 techniques: gas chromatography with flame ionization detector, thermal conductivity detector,  
328 quadrupole mass spectrometry, hydrogen peroxide analyser, Fourier transform infrared  
329 spectrometry, liquid chromatography and high-resolution mass spectrometry (Orbitrap Q-  
330 Exactive). H/D exchange with  $D_2O$  was used to assess the presence of hydroxyl or hydroperoxyl  
331 groups in the products. The large set of qualitative and quantitative data obtained here was  
332 combined with published results obtained under the same experimental conditions at 1 atm, and  
333 simulated. A kinetic reaction mechanism which takes into account the Korcek mechanism was  
334 taken from the literature and used to simulate the present experiments. Reaction pathway  
335 analyses revealed that in the model the reactions of the Korcek mechanism are mostly  
336 contributing to the formation of formic acid, acetic acid, and acetone at 1 and 10 atm, but not  
337 acetaldehyde. This study showed that the selected kinetic model only partially represents the  
338 data and should be improved, both under cool flame and high temperature conditions. For future  
339 kinetic modelling, one should quantify the highly oxidized products detected by FIA/UHPLC-  
340 Orbitrap. This is a very challenging task since such products needed to calibrate the instruments  
341 are not commercially available and their synthesis is difficult.

342

## 343 **Acknowledgements**

344 Support from the CAPRYSES project (ANR- 11-LABX-006–01) funded by ANR through  
345 the PIA (Programme d'Investissement d'Avenir) is gratefully acknowledged. Help from C.  
346 Togbé and F. Karsenty for the 10 atm JSR experiments is gratefully acknowledged.

347

## 348 **References**

- 349 [1] Guibet, JC, Fuels and Engines. Technology - Energy - Environment. Editions Technip: Paris, 1999, p.  
350 786.  
351 [2] Speight, J, in: J. Speight (Ed.) Shale Oil and Gas Production Processes, Gulf Professional Publishing:  
352 2020.



- 353 [3] Xu, Q, Liu, BZ, Chen, WY, Yu, TP, Zhang, ZH, Zhang, C, Wei, LX, Wang, ZD, Comprehensive study  
354 of the low-temperature oxidation chemistry by synchrotron photoionization mass spectrometry and gas  
355 chromatography. *Combust. Flame* 2022; 236: 11797-11797.
- 356 [4] Djehiche, M, Le Tan, NL, Jain, CD, Dayma, G, Dagaut, P, Chauveau, C, Pillier, L, Tomas, A,  
357 Quantitative Measurements of HO<sub>2</sub> and Other Products of n-Butane Oxidation (H<sub>2</sub>O<sub>2</sub>, H<sub>2</sub>O, CH<sub>2</sub>O,  
358 and C<sub>2</sub>H<sub>4</sub>) at Elevated Temperatures by Direct Coupling of a Jet-Stirred Reactor with Sampling Nozzle  
359 and Cavity Ring-Down Spectroscopy (cw-CRDS). *J. Am. Chem. Soc.* 2014; 136: 16689-16694.
- 360 [5] Bahrini, C, Morajkar, P, Schoemaeker, C, Frottier, O, Herbinet, O, Glaude, P-A, Battin-Leclerc, F,  
361 Fittschen, C, Experimental and modeling study of the oxidation of n-butane in a jet stirred reactor using  
362 cw-CRDS measurements. *Phys. Chem. Chem. Phys.* 2013; 15: 19686-19698.
- 363 [6] Bahrini, C, Herbinet, O, Glaude, PA, Schoemaeker, C, Fittschen, C, Battin-Leclerc, F, Quantification  
364 of Hydrogen Peroxide during the Low-Temperature Oxidation of Alkanes. *J. Am. Chem. Soc.* 2012;  
365 134: 11944-11947.
- 366 [7] Herbinet, O, Battin-Leclerc, F, Bax, S, Le Gall, H, Glaude, P-A, Fournet, R, Zhou, Z, Deng, L, Guo, H,  
367 Xie, M, Qi, F, Detailed product analysis during the low temperature oxidation of n-butane. *Phys. Chem.*  
368 *Chem. Phys.* 2011; 13: 296-308.
- 369 [8] Blocquet, M, Schoemaeker, C, Amedro, D, Herbinet, O, Battin-Leclerc, F, Fittschen, C, Quantification  
370 of OH and HO<sub>2</sub> radicals during the low-temperature oxidation of hydrocarbons by Fluorescence Assay  
371 by Gas Expansion technique. *Proc. Natl. Acad. Sci. U. S. A.* 2013; 110: 20014-20017.
- 372 [9] Battin-Leclerc, F, Herbinet, O, Glaude, P-A, Fournet, R, Zhou, Z, Deng, L, Guo, H, Xie, M, Qi, F, New  
373 experimental evidences about the formation and consumption of ketohydroperoxides. *Proc. Combust.*  
374 *Inst.* 2011; 33: 325-331.
- 375 [10] Ranzi, E, Cavallotti, C, Cuoci, A, Frassoldati, A, Pelucchi, M, Faravelli, T, New reaction classes in the  
376 kinetic modeling of low temperature oxidation of n-alkanes. *Combust. Flame* 2015; 162: 1679-1691.
- 377 [11] Jalan, A, Alecu, IM, Meana-Paneda, R, Aguilera-Iparraguirre, J, Yang, KR, Merchant, SS, Truhlar, DG,  
378 Green, WH, New Pathways for Formation of Acids and Carbonyl Products in Low-Temperature  
379 Oxidation: The Korcek Decomposition of gamma-Ketohydroperoxides. *J. Am. Chem. Soc.* 2013; 135:  
380 11100-11114.
- 381 [12] Zinbo, M, Jensen, RK, Korcek, S, Gas-liquid-chromatography of oxygenated compounds related to  
382 autoxidation of n-hexadecane. *Anal. Lett.* 1977; 10: 119-132.
- 383 [13] Jensen, RK, Korcek, S, Mahoney, LR, Zinbo, M, Liquid-phase autoxidation of organic-compounds at  
384 elevated-temperatures .1. stirred flow reactor technique and analysis of primary products from normal-  
385 hexadecane autoxidation at 120-degrees-C 180-degrees-C. *J. Am. Chem. Soc.* 1979; 101: 7574-7584.
- 386 [14] Jensen, RK, Korcek, S, Mahoney, LR, Zinbo, M, Liquid-phase autoxidation of organic-compounds at  
387 elevated-temperatures .2. Kinetics and mechanisms of the formation of cleavage products in normal-  
388 hexadecane autoxidation. *J. Am. Chem. Soc.* 1981; 103: 1742-1749.
- 389 [15] Jensen, RK, Zinbo, M, Korcek, S, HPLC determination of hydroperoxidic products formed in the  
390 autoxidation of normal-hexadecane at elevated-temperatures. *J. Chromatogr. Sci.* 1983; 21: 394-397.
- 391 [16] Popolan-Vaida, DM, Eskola, AJ, Rotavera, B, Lockyear, JF, Wang, ZD, Sarathy, SM, Caravan, RL,  
392 Zador, J, Sheps, L, Lucassen, A, Moshhammer, K, Dagaut, P, Osborn, DL, Hansen, N, Leone, SR,  
393 Taatjes, CA, Formation of Organic Acids and Carbonyl Compounds in n-Butane Oxidation via gamma-  
394 Ketohydroperoxide Decomposition. *Angewandte Chemie-International Edition* 2022; 61: 9168-9168.
- 395 [17] Wang, Z, Popolan-Vaida, DM, Chen, B, Moshhammer, K, Mohamed, SY, Wang, H, Sioud, S, Raji, MA,  
396 Kohse-Höinghaus, K, Hansen, N, Dagaut, P, Leone, SR, Sarathy, SM, Unraveling the structure and  
397 chemical mechanisms of highly oxygenated intermediates in oxidation of organic compounds.  
398 *Proceedings of the National Academy of Sciences* 2017; 114: 13102-13107.
- 399 [18] Belhadj, N, Benoit, R, Dagaut, P, Lailliau, M, Serinyel, Z, Dayma, G, Khaled, F, Moreau, B, Foucher,  
400 F, Oxidation of di-n-butyl ether: Experimental characterization of low-temperature products in JSR and  
401 RCM. *Combust. Flame* 2020; 222: 133-144.
- 402 [19] Belhadj, N, Benoit, R, Dagaut, P, Lailliau, M, Experimental characterization of n-heptane low-  
403 temperature oxidation products including keto-hydroperoxides and highly oxygenated organic  
404 molecules (HOMs). *Combust. Flame* 2021; 224: 83-93.
- 405 [20] Belhadj, N, Benoit, R, Dagaut, P, Lailliau, M, Experimental Characterization of Tetrahydrofuran Low-  
406 Temperature Oxidation Products Including Ketohydroperoxides and Highly Oxygenated Molecules.  
407 *Energy Fuels* 2021; 35: 7242-7252.
- 408 [21] Belhadj, N, Benoit, R, Dagaut, P, Lailliau, M, Moreau, B, Foucher, F, Low-temperature oxidation of a  
409 gasoline surrogate: Experimental investigation in JSR and RCM using high-resolution mass  
410 spectrometry. *Combust. Flame* 2021; 228: 128-141.
- 411 [22] Belhadj, N, Benoit, R, Dagaut, P, Lailliau, M, Serinyel, Z, Dayma, G, Oxidation of di-n-propyl ether:  
412 Characterization of low-temperature products. *Proc. Combust. Inst.* 2021; 38: 337-344.

- 413 [23] Belhadj, N, Benoit, R, Lailliau, M, Glasziou, V, Dagaut, P, Oxidation of diethyl ether: Extensive  
414 characterization of products formed at low temperature using high resolution mass spectrometry.  
415 *Combust. Flame* 2021; 228: 340-350.
- 416 [24] Belhadj, N, Lailliau, M, Benoit, R, Dagaut, P, Experimental and kinetic modeling study of n-hexane  
417 oxidation. Detection of complex low-temperature products using high-resolution mass spectrometry.  
418 *Combust. Flame* 2021; 233: 111581.
- 419 [25] Belhadj, N, Lailliau, M, Benoit, R, Dagaut, P, Towards a Comprehensive Characterization of the Low-  
420 Temperature Autoxidation of Di-n-Butyl Ether. *Molecules* 2021; 26: 7174.
- 421 [26] Belhadj, N, Lailliau, M, Benoit, R, Dagaut, P, Experimental and kinetic modeling study of n-pentane  
422 oxidation at 10 atm, Detection of complex low-temperature products by Q-Exactive Orbitrap. *Combust.*  
423 *Flame* 2022; 235: 11723-11723.
- 424 [27] Belhadj, N, Lailliau, M, Dbouk, Z, Benoit, R, Moreau, B, Foucher, F, Dagaut, P, Gasoline Surrogate  
425 Oxidation in a Motored Engine, a JSR, and an RCM: Characterization of Cool-Flame Products by High-  
426 Resolution Mass Spectrometry. *Energy Fuels* 2022; 36: 3893-3908.
- 427 [28] Chen, W, Xu, Q, Lou, H, Di, Q, Xie, C, Liu, B, Yang, J, Gall, HL, Tran, LS, Wang, X, Xia, Z,  
428 Herbinet, O, Battin-Leclerc, F, Wang, Z, Variable pressure JSR study of low temperature oxidation  
429 chemistry of n-heptane by synchrotron photoionization mass spectrometry. *Combust. Flame* 2022; 240:  
430 111946.
- 431 [29] Dagaut, P, Cathonnet, M, Rouan, JP, Foulatier, R, Quilgars, A, Boettner, JC, Gaillard, F, James, H, A  
432 jet-stirred reactor for kinetic studies of homogeneous gas-phase reactions at pressures up to ten  
433 atmospheres ( $\approx 1$  MPa). *Journal of Physics E: Scientific Instruments* 1986; 19: 207-209.
- 434 [30] Dagaut, P, Cathonnet, M, Boettner, JC, Gaillard, F, Kinetic modeling of ethylene oxidation. *Combust.*  
435 *Flame* 1988; 71: 295-312.
- 436 [31] Le Cong, T, Dagaut, P, Dayma, G, Oxidation of Natural Gas, Natural Gas/Syngas Mixtures, and Effect  
437 of Burnt Gas Recirculation: Experimental and Detailed Kinetic Modeling. *Journal of Engineering for*  
438 *Gas Turbines and Power* 2008; 130: 041502-10.
- 439 [32] Tao, T, Kang, SQ, Sun, WY, Wang, JX, Liao, HD, Moshhammer, K, Hansen, N, Law, CK, Yang, B, A  
440 further experimental and modeling study of acetaldehyde combustion kinetics. *Combust. Flame* 2018;  
441 196: 337-350.
- 442 [33] Sun, W, Tao, T, Lailliau, M, Hansen, N, Yang, B, Dagaut, P, Exploration of the oxidation chemistry of  
443 dimethoxymethane: Jet-stirred reactor experiments and kinetic modeling. *Combust. Flame* 2018; 193:  
444 491-501.
- 445 [34] Moshhammer, K, Jasper, AW, Popolan-Vaida, DM, Wang, ZD, Shankar, VSB, Ruwe, L, Taatjes, CA,  
446 Dagaut, P, Hansen, N, Quantification of the Keto-Hydroperoxide (HOOCH<sub>2</sub>OCHO) and Other Elusive  
447 Intermediates during Low-Temperature Oxidation of Dimethyl Ether. *J. Phys. Chem. A* 2016; 120:  
448 7890-7901.
- 449 [35] Moshhammer, K, Jasper, AW, Popolan-Vaida, DM, Lucassen, A, Dievert, P, Selim, H, Eskola, AJ,  
450 Taatjes, CA, Leone, SR, Sarathy, SM, Ju, YG, Dagaut, P, Kohse-Hoinghaus, K, Hansen, N, Detection  
451 and Identification of the Keto-Hydroperoxide (HOOCH<sub>2</sub>OCHO) and Other Intermediates during Low-  
452 Temperature Oxidation of Dimethyl Ether. *J. Phys. Chem. A* 2015; 119: 7361-7374.
- 453 [36] "ANSYS CHEMKIN 20.0", ANSYS Reaction Design: 2020.
- 454 [37] Schofield, K, The enigmatic mechanism of the flame ionization detector: Its overlooked implications  
455 for fossil fuel combustion modeling. *Prog. Energy Combust. Sci.* 2008; 34: 330-350.
- 456 [38] Serinyel, Z, Lailliau, M, Thion, S, Dayma, G, Dagaut, P, An experimental chemical kinetic study of the  
457 oxidation of diethyl ether in a jet-stirred reactor and comprehensive modeling. *Combust. Flame* 2018;  
458 193: 453-462.

460